



<b>Title</b>	Correlating in-situ process monitoring data with the reduction in load bearing capacity of selective laser melted Ti-6Al-4V porous biomaterials
<b>Authors(s)</b>	Egan, Darragh S., Dowling, Denis P.
<b>Publication date</b>	2020-06
<b>Publication information</b>	Egan, Darragh S., and Denis P. Dowling. "Correlating In-Situ Process Monitoring Data with the Reduction in Load Bearing Capacity of Selective Laser Melted Ti-6Al-4V Porous Biomaterials." Elsevier, June 2020. <a href="https://doi.org/10.1016/j.jmbbm.2020.103723">https://doi.org/10.1016/j.jmbbm.2020.103723</a> .
<b>Publisher</b>	Elsevier
<b>Item record/more information</b>	<a href="http://hdl.handle.net/10197/11941">http://hdl.handle.net/10197/11941</a>
<b>Publisher's statement</b>	This is the author's version of a work that was accepted for publication in Journal of the Mechanical Behavior of Biomedical Materials. Changes resulting from the publishing process, such as peer review, editing, corrections, structural formatting, and other quality control mechanisms may not be reflected in this document. Changes may have been made to this work since it was submitted for publication. A definitive version was subsequently published in Journal of the Mechanical Behavior of Biomedical Materials (106, Article Number: 103723, (2020)) <a href="https://doi.org/10.1016/j.jmbbm.2020.103723">https://doi.org/10.1016/j.jmbbm.2020.103723</a>
<b>Publisher's version (DOI)</b>	<a href="https://doi.org/10.1016/j.jmbbm.2020.103723">10.1016/j.jmbbm.2020.103723</a>

Downloaded 2025-12-04 23:07:10

The UCD community has made this article openly available. Please share how this access benefits you. Your story matters! (@ucd\_oa)



© Some rights reserved. For more information

# CORRELATING IN-SITU PROCESS MONITORING DATA WITH THE REDUCTION IN LOAD BEARING CAPACITY OF SELECTIVE LASER MELTED Ti-6Al-4V POROUS BIOMATERIALS

Darragh S. Egan<sup>1</sup>, Denis P. Dowling<sup>1</sup>

<sup>1</sup> I-Form Advanced Manufacturing Research Centre, University College Dublin, Belfield, Dublin. 4, Ireland.

Corresponding author: darragh.egan@i-form.ie. University College Dublin, Dublin, Ireland.

## ABSTRACT

Selective Laser Melting allows for the creation of intricate porous structures, that possess favourable biological properties. These structures are known as porous biomaterials. The focus of this paper is to evaluate the use of an in-line photodiode based process monitoring system, for the monitoring of the operational behaviour of the laser, and to correlate this with the resultant parts mechanical performance.

In this study the production scale Renishaw 500M was used to produce porous structures, using Ti-6Al-4V feedstock powder. During the process, a co-axial process monitoring system was utilised to generate data relating to both the meltpool and the operational behaviour of the laser. An advanced scanning technique was used to produce the structures, whereby the laser parameters determine the strut dimensions. In this study, the laser input energy was reduced by 33%, 66% and 100%, at specific layers within the structures. Computer Tomography and Scanning Electron Microscopy was utilised to characterise the affected struts within the structures, while quasi-static compression testing was used to determine the structure's mechanical properties.

It was demonstrated that as the level of input energy decreased and the number of affected layers increased, a corresponding decrease in the load bearing capacity of the structures occurred. With the structures experiencing a significant loss in strength also exhibiting a change in the failure mode during compression testing. Data generated during the processing of such structures was compared to the data generated during the processing of control structures, with the difference between the two been calculated on a layer-by-layer basis. A clear correlation was demonstrated between the total level of deviation between the two signal sets and a reduction in the load bearing capacity of the structures. This indicates that by comparing build data to a benchmark data set, valuable information relating to the structural integrity of the porous structures can be obtained.

# 1 INTRODUCTION

Selective Laser Melting (SLM), allows for the production of porous metallic scaffolds, composed of internal micro-scaled architectures, with controlled porosity, strut and pore diameter. This in turn allows for the creation of porous meta-biomaterials with controlled, site specific mechanical properties [1]. These porous structures have a number of advantageous properties, including high strength to weight ratios, tuneable mechanical properties, as well as possessing osteoconductive features [2][3][4]. Combining both the freeform geometries that SLM can create, and the advantageous biological properties of these structures, extensive research has been carried out on the use of these porous-biomaterials as bone replacement implants.

A number of studies have been carried out to assess the effect of SLM processing parameters on the mechanical properties of Ti-6Al-4V samples. Khorasania et al. for example, studied the effect of heat treatment, laser power, scan speed, hatch spacing and scan angle on the mechanical properties of bulk Ti-6Al-4V samples [5]. These processing parameters were correlated with the porosity and hardness of the samples. Xu et al. also investigated processing parameters on the alloys microstructure [6]. In their work it was shown that through process parameter optimisation, the undesirable martensitic microstructure could be transformed to a more favourable ultrafine lamellar ( $\alpha+\beta$ ) structure. This more favourable microstructure resulted in an increase in the elongation at failure, with values of 11.4% reported. In addition to the mechanical and microstructural properties of SLM Ti-6Al-4V, Kaschel et al. also investigated their influence on part dimensions [7]. It was demonstrated that lower laser power, 250 W resulted in a 2% deviation between the CAD and the as-built part geometry, this increased to 4% when a power of 400 W, was applied. Indicating that in addition to porosity and hardness, that processing parameters can also influence the geometric accuracy of parts produced using the SLM technology.

Melancon et al. [8] investigated the relationship between biomaterial micro-architecture and the mechanical properties of porous structures. Experiments utilising computer tomography, mechanical testing and statistical analysis of geometric defects were used to improve the accuracy of property maps for two different types of biomaterials. While this study took into account the effect that micro-defects had on the accuracy of predictive models, the effect that more severe defects, that could potentially lead to a reduction in part quality, was not assessed. Bobbert et al. reported on the design and SLM of sixteen different types of porous biomaterials, which exhibited mechanical properties similar to that of human trabecular and cortical bone.

The biomaterials created were reported to possess mechanical properties which reduced potential stress shielding, while maintaining a sufficiently open structure to promote bone ingrowth [9].

An important mechanical property of a bone scaffold of implant is its fatigue performance. Dallago et al. assessed the fatigue strength of regular cubic open cellular structures, each with a Young's modulus of 3 GPa, which is similar to that of human trabecular bone. In their study the effect of defects such as porosity, surface roughness and geometric inaccuracies on the fatigue life of the structures was investigated. Dallago et al. found that the fatigue strength of the structures was highly dependent on imperfections and notches on the surface of the structures [10]. Extensive research has been carried out exploring the design, topology optimisation of porous structures, as well as on the effects that these properties have on the biological properties of the structures [11][12][13][14][15][16][17][18][19][20][21]. There have been no reports however, investigating the SLM process of porous biomaterials from a quality control or quality assurance point of view.

Despite the many advantages of SLM, issues surrounding the consistency of parts produced necessitates a high level of post build quality control (QC), in order to ensure that the parts meet their specific requirements [22]. QC checks, such as computer tomography (CT) scanning, are usually carried out post build on every part, of a given build [23]. This method of QC is both expensive and time consuming, with parts that fail to meet the required specifications been scrapped, generating more process waste [24]. Therefore, in order to reduce the amount of post build QC, it is critical to develop 'robust' methods of in-process monitoring for the identification of build defects.

A number of authors have reported on the use of monitoring (PM) systems for SLM processes, [25][26][27][28]. These typically involved the use of photodiode systems to monitor the emissions coming from the meltpool created during the processing of single line scans or relatively primitive test samples. There have been very few reports on how the data generated by PM systems correlated with the part's mechanical properties. An example by Bisht et. al. [29], involved the use of a reduced flow of shielding gas in order to produce sub-optimal parts. In their work the PM system generated a colour map illustrating the level of emissions created during the processing of Ti-6Al-4V tensile bars. Any abrupt change in the level of emissions at a given point that occurred on consecutive layers was deemed an "event". A strong correlation was demonstrated between the increasing volume of "events" and a reduction in the parts mechanical properties [29]. The method of analysis however was manual and therefore does not facilitate real-time process control.

In this study the aim is to apply in-situ process monitoring during the SLM of porous structures. The aim is to assess the effect on lattice mechanical performance, of incorporating layers within the part, which were processed with a reduction in laser power. The reduction in input energy was monitored using a photodiode based monitoring system. The reduction in signal intensity detected was compared with ‘control’ layers, for which no reduction in laser energy had been applied. Specifically, the objectives of this study are to:

- Assess how both the number of layers and the level of laser power reduction effect both the process monitoring data generated and the load bearing strength of the as-built porous biomaterials.
- Determine whether or not a correlation exists between the level of deviation between the control data and the build data, with a reduction in part strength.

## 2 EXPERIMENTAL SETUP

### 2.1 MATERIAL & MACHINE SETUP

All samples were produced using a Renishaw RenAM500M, fitted with an in-situ process monitoring (PM) system. This system utilises a 500 W laser ( $\lambda = 1.07 \mu\text{m}$ ), with an in focused spot size of around  $80 \mu\text{m}$  in diameter. The RenAM500M can operate in both continuous laser mode and in a modulated mode. In the latter, the laser fires for a pre-defined amount of time following which the laser is switched off and moves a defined distance to the next point location, before firing again for the user defined time, known as the exposure time. During this study all sample parts were created using the modulated laser mode. All test pieces were fabricated using Ti-6Al-4V grade 23 powder, obtained from AP & C, with powder particle diameters in the range of  $15$  to  $45 \mu\text{m}$ . Prior to the build commencing, a vacuum was used to remove the level of oxygen in the chamber, following which argon gas was introduced to achieve an inert atmosphere. During processing the build platform was maintained at a temperature of  $170^\circ\text{C}$ . The InfiniAM Spectral process monitoring (PM) system uses a number of photodiodes to obtain data relating to the plasma and IR emissions generated by the meltpools, during the build process. Along with this data, data relating to the operational behaviour of the laser is also generated [30]. Feedback on the laser energy input is provided through the LaserView module, while the level of emissions emitted from the meltpool during processing is obtained through the MeltView module. The data is recorded, at  $100 \text{ kHz}$ , and can then reconstructed into both 2D and 3D views in near real time [30].

## 2.2 TEST SPECIMENS

Diamond based non-stochastic unit cell structures were selected as the focus of this study. Firstly due to their close packing density they have potential applications for use as porous biomaterials. Secondly, due to the relative ease with which the unit cell geometry can be produced using SLM. Finally, this work aims to build on a previous study, in which a process parameter-process signature-part quality relationship for diamond based non-stochastic structures was demonstrated [31]. In this current study the porous structures were created using the single exposure method of fabrication. In this method of fabrication the process parameters, namely the beam diameter, the laser power and the exposure time determine the diameter of the struts created and therefor control the overall strength of the structure, as demonstrated in [31]. For this method of fabrication each meltpool created will form one layer of a given strut. For this reason it is critical that each meltpool is formed correctly. The resultant porous structures are thus extremely sensitive to imperfections in the meltpool. Any abnormal meltpool could result in a defective strut, which in turn could have a serious adverse influence on the load bearing capacity of the overall structure. Due to the manner in which these samples are formed, using the single exposure method, it is anticipated that the reduced input energy layers will result in struts forming with a reduction in strut diameter, compared to the control samples.

The test specimen used in this work consisted of a (L x W x H) 15x15x28 mm lattice structure, composed of 1.5 mm diamond unit cells. The structure created conformed to ISO 13314, the ISO standard describing the method of compression testing of porous metallic structures. After the build process, samples were removed from the build plate and cut, using a precision saw, to 20 mm in height. Following this, all samples were washed in an ultrasonic bath and dried. No post build heat treatment was carried out on the as-built structures.

For this study all structures were created using the single exposure method, where by the process parameters determine the strut diameter. In this study an exposure time and laser power of 750  $\mu$ s and 150 W were utilised respectively, at a layer height of 30  $\mu$ m.

The control samples used in this work were processed using these parameters throughout the entire structure, while the other test samples were created containing layers with reduced input laser power. This was done by reducing the laser power at specific layers within the structures. The laser power was intentionally reduced in an attempt to affect the structural integrity of the sample and to induce a difference in the process monitoring data generated, compared to

the control sample. This, according to Sharratt [32], is representative of an equipment induced defects.

To assess the sensitivity of the PM system and the mechanical properties of the structures to layers processed with low input power, the number of affected layers was varied between 1, 3, 5, 7 and 9, referred to as V1, V3, V5, V7 and V9 in the text that follows. Further to this, to assess the sensitivity of the PM system and the mechanical response of the structures to varying levels of power reduction, three batches of samples were created, each with an increased level of laser power reduction. In the first batch of low input energy samples, an energy reduction of 33 % was used, referred to as the S1 sample batch. The second and third batches of samples an energy reduction of 66 % and 100 % were utilised, referred to as S2 and S3 respectively.

In the following text samples have a notation of SxVy, where x indicates the level of energy reduction and y indicates the number of effected layers, as detailed in

Table 1. For example, the S2V9 sample is fabricated with a 66 % reduction in input energy, over 9 consecutive layers. The aim of designing samples in this manner was to assess the effect that a reduction in laser power, over a range of layers, has on the PM data generated and on the mechanical response of the structures. These samples are also representative of what might arise if a laser malfunction occurred, resulting in the laser not operating at the required level, potentially resulting in laser power induced defects occurring.

*Table 1: Notation associated with each test sample produced in this study. Where the S value indicates the level of reduction in laser power for the number of layers given by the V value*

<b>REDUCTION IN LASER POWER</b>			
<b>NO. OF LAYERS</b>	<b>33%</b>	<b>66%</b>	<b>100%</b>
<b>1</b>	S1V1	S2V1	S3V1
<b>3</b>	S1V3	S2V3	S3V3
<b>5</b>	S1V5	S2V5	S3V5
<b>7</b>	S1V7	S2V7	S3V7
<b>9</b>	S1V9	S2V9	S3V9*

\*It was found that it was not possible to build the S3V9 test sample due the high number of layers with no input energy, therefor this sample was not included in the build analysis. As a result, 15 sample types, including the control sample set, were examined, each with a sample size of n=4.

## 2.3 DATA ACQUISITION AND ANALYSIS

During the SLM processes, the process monitoring system was utilised to gather data at a rate of 100 kHz. The system uses one photodiode to provide feedback on the laser energy input and two photodiodes to provide information about the emissions emitted from the meltpool and the plasma created during the SLM process. The data is then used to construct either a 2D or 3D representation of the part, in near real time, as described in [30].

In this study, analysis was carried out after the build was completed on the raw data generated during the processing of each individual sample created. The data associated with each sample was plotted as a function of build plate location. A region of interest (ROI), 16x16mm, was then taken around each structure. The signal generated within each ROI was then analysed on a layer-by-layer basis, using the Matlab R2019a software.

For each of the three photodiodes five data points were generated, they were; (i) the mean, (ii) the maximum, (iii) the minimum, (iv) the standard deviation and (v) the sum. The Sum value is the total sum of the PD signal generated per layer of each lattice structure. With 5 data points been created for each of the three photodiodes, 15 different data sets were created. This resulted in over 14,265 data points been obtained per sample (951 layers x 3 photodiodes x 5 recordings each= 14,265), with 60 samples a total of 855,900 data points were generated. This resulted 350 MB of data to be analysed. As the first 8 mm of the build acted as support material, and were subsequently removed during the sample preparation stages, the data corresponding to these layers was also omitted from analysis. This resulted in a total of 665 layers (~20 mm) been analysed. Out of the 665 layers analysed, the number of layers containing reduced input energy layers represented between 0.15% and 1.35 % of the total layers.

### 2.3.1 Control vs build data

The 15 different data sets generated by the control samples were taken as a baseline in this study. The data generated during the processing of each of the structures, outlined in Table 1, was compared to the corresponding baseline data set, on a layer-by-layer basis. The percentage deviation that occurred between each was also calculated. In order to allow for some acceptable signal deviation, the maximum variance that occurred within the each of the baseline data sets was taken as the upper and lower limits of acceptance. When the deviation between the build data and the baseline data fell within the acceptable limits, the deviation value was not included in any further analysis. Finally, to quantify the effect that the layers with reduced laser power had on the PM data generated by each sample, the deviation that occurred between each of the



baseline data sets and the corresponding build data sets was summed together to give a Total Signal Deviation (TSD).

## 2.4 CHARACTERISATION

To assess the effect that the layers with lower input energy had on the load bearing capacity of the porous structures, samples were mechanically tested according to ISO 13314. Samples were tested using a Tinius Olsen 50 kN machine, equipped with a 50 kN load cell. A strain rate of  $\sim 10^{-2}$  strain/second was used in order to comply to the ISO 13314 specifications. Testing concluded after the first maximum compressive load and true elastic gradient of each of the samples was obtained. Prior to testing, a frame stiffness correction program was run 5 times on the mechanical tester. This allowed for the stiffness of the mechanical tester to be taken into account when calculating the strain measurements.

Computed tomography measurements were obtained using a Phoenix Nanotom |m| system. This facilitated structural information relating to the structures to be obtained. Each scan was carried out over approximately 9 minutes at 100 kV and 200  $\mu$ A. A resolution of approx. 7  $\mu$ m was achieved. The processing of the CT data was carried out using VG studio Max 3.3. The resulting data was used to obtain detailed images of the struts morphology.

Further examination of the struts was carried out using a Hitachi EM4000Plus SEM, which facilitated information relating to the diameter of the struts to be obtained.

## 3 RESULTS & DISCUSSION

This section firstly details the effect of reducing the laser power during the build process, on the photodiode data obtained. This is followed by a detailed review of the effect of systematically altering laser power on the compressive strength of the resultant porous structures. Except where otherwise stated, only the average signal (generated by the  $n=4$  samples for each sample type) is shown, for ease of interpretation. Note, a number of results contain colour images, readers are directed to the electronic version for representation.

### 3.1 CONTROL DATA & STRUCTURE

Figure 1 (top) shows the average, maximum and minimum of the mean photodiode (PD) signal generated by PM system during the processing of the control samples used in this study. For clarity only a selection of layers is shown. Due to the periodic repeating nature of the structures geometry, a repeating trend is observed in the data generated. It can be seen from this figure

that despite the parts been produced across different locations on the build plate, there is very little difference between the average, the maximum and minimum PD signal obtained.

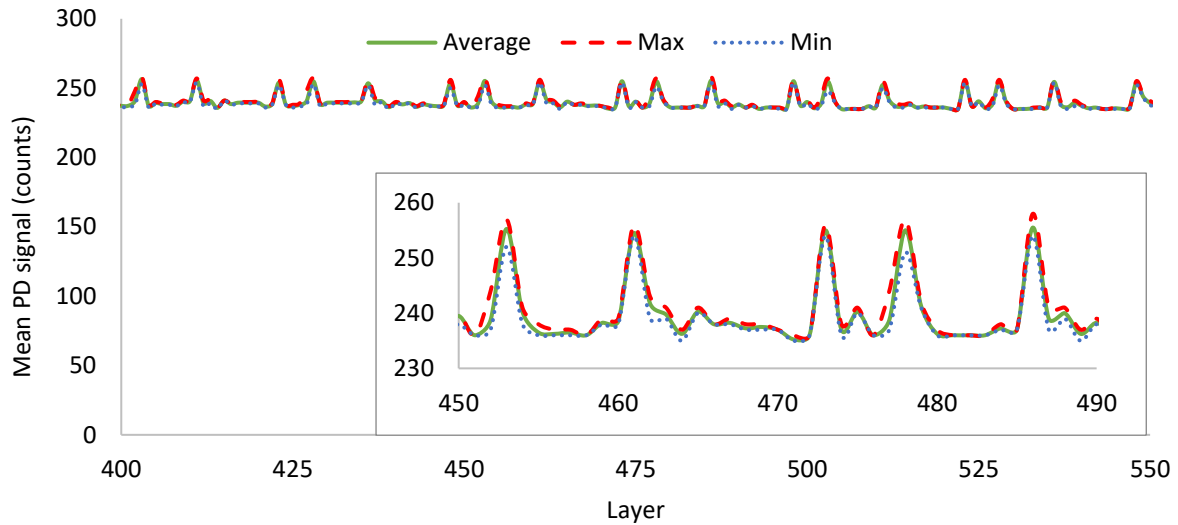


Figure 1: Photodiode data generated during the processing of all the 'control' samples layers 400 to 550. Insert: Detailed view of layers 450 to 490 demonstrating the closeness of the data generated between the maximum and minimum PD signals.

A maximum difference of 3.1 % was recorded between the average and the maximum signal detected, while a maximum difference of 3.4 % was recorded between the average and the minimum signal detected. This low variance indicates that the laser operated consistently across the build plate and throughout the entire build process. The 3.1 and 3.4 % variance recorded between the control data set was then set as the acceptable limits in the remainder of this study. Where deviation between the control data and the build data fell within these limits the deviation value was set to zero. This resulted in any minor deviations between the data sets been omitted from further analysis. The repeating nature of the signal seen in this figure occurs due to the periodically repeating nature of the geometry of the non-stochastic diamond unit cells that make up the structure. The high values obtained (~255 counts) in this figure correspond to layers where node junctions occurred. At these layers an increased amount of exposure points occurred compared to the layers containing just the individual struts. This can be seen in Figure 2 centre, where the yellow arrow points to the single exposure points within the struts, while the red arrow points to the exposure points within the node junction.

In a previous study it was demonstrated that the laser parameters control the resultant strut diameter, with increasing input energy resulting in increased strut diameters [31]. The struts formed within the control samples in this study, processed with 150 W and 750  $\mu$ s, can be seen in Figure 2 right.

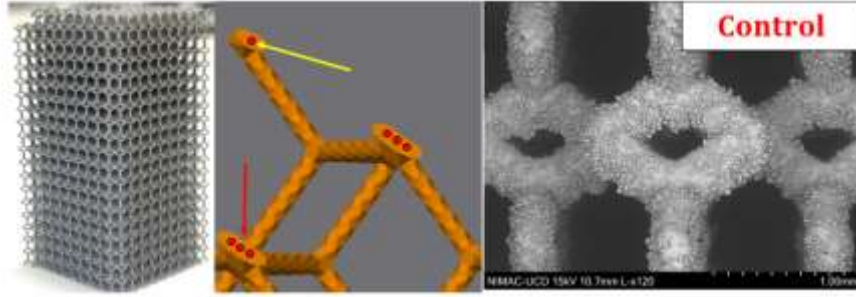


Figure 2: Left: Macro image of the as built structure. Centre: Image of CAD file of a lattice structure. Yellow arrow pointing to the single exposure point within the struts. Red arrow points to the exposure points at the node junctions, image taken from the QuantAM build preparation software. Right: SEM image of the struts within the control sample.

### 3.2 INFLUENCE OF ENERGY REDUCTION ON THE PROCESS MONITORING DATA

Figure 3 demonstrates the effect that reducing the laser energy from S1 to S3, had on the mean PD signal generated, while processing only a single layer. The result of decreasing the energy input by 33%, 66% and 100 %, was a decrease in the mean PD signal generated, from 245 counts for the control, to 156, 86 and 2 counts, respectively. Similar recordings were observed at each of the affected layers when the number of reduced input energy layers was increased. For the S1 and S2 samples, this is representative of what might be recorded if the laser did not behave as intended and reduction in laser input energy occurred. A 100% reduction in input energy during processing could for example, represent what might be detected if the laser failed to fire on a given layer or alternatively if a slicing or scan path error occurred, resulting in the laser not scanning a layer(s) of a part.

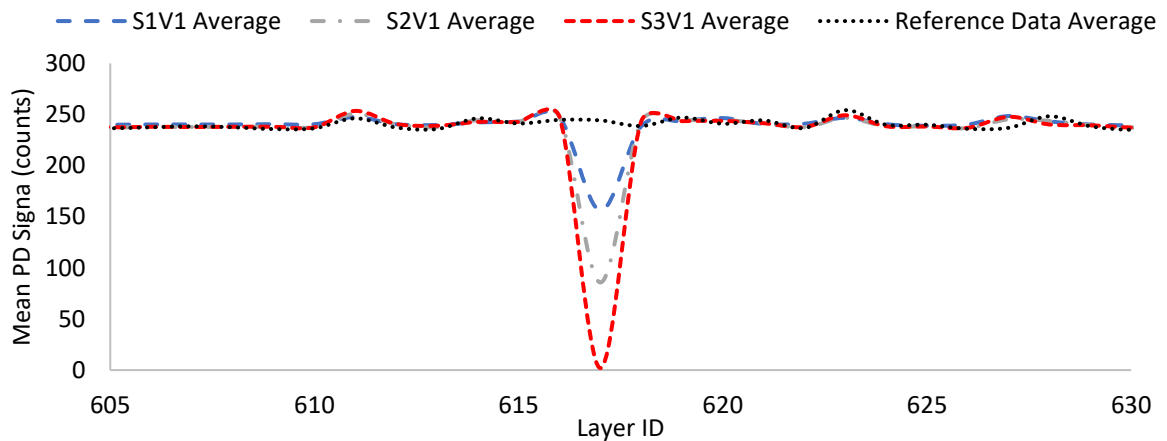


Figure 3: Effect of reducing the energy input, at one layer, on PD response.

Figure 4 shows the deviation between the control data set and the data generated from each of the lattice structures containing layers with reduced input energy, over a selected range of layers. From this graph it appears that as the number of low input energy layers increased, at a fixed energy input, then the signal intensity remains at a constant deviation throughout each of the respective layers. When the level of energy input is further reduced the deviation between

the control data and the build data increases, as detailed earlier. The deviation that occurred for each of the S1, S2 and S3 samples was approximately 33%, 66% and 99 % respectively, which corresponds directly to the level of energy input reduction that was associated with sample. This result demonstrates the ability of the in-situ monitoring systems to detect variations in the laser input, which could be potentially used to detect laser induced defects.

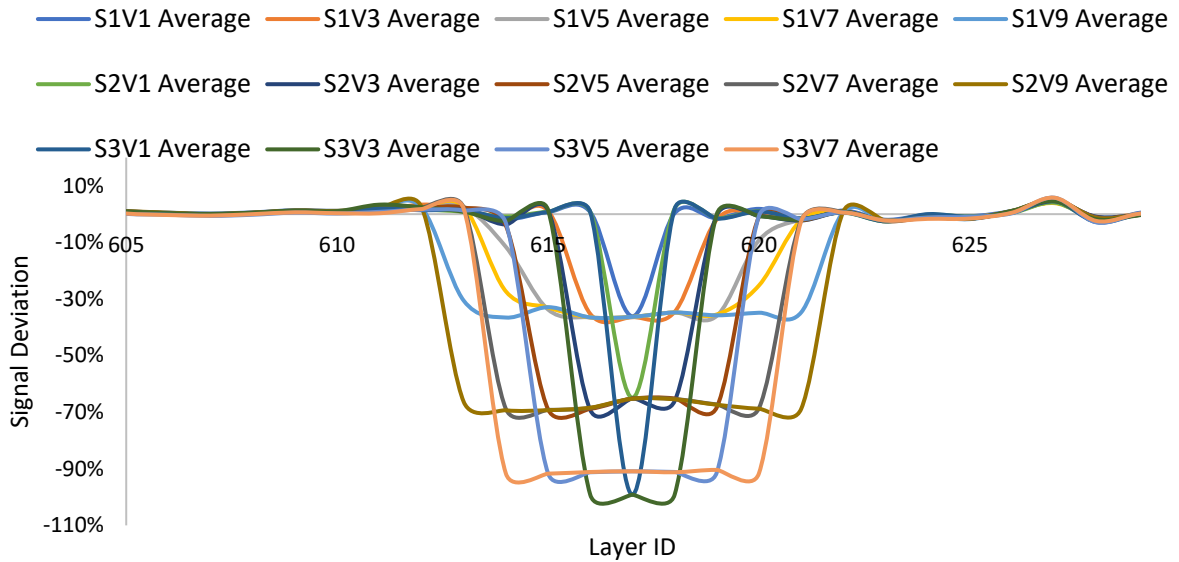


Figure 4: Effect of energy reduction level and the number of effected layers on the deviation between build data and the control data. For colour interpretation readers should see the online version.

### 3.3 INFLUENCE OF ENERGY REDUCTION ON THE MECHANICAL RESPONSE OF THE POROUS STRUCTURES

In order to evaluate the effect of reducing the laser energy, the total signal deviation (TSD) was calculated, this sums together the percentage deviation that occurred at every layer within the structures, thereby providing an indication as to the effect that the low input energy layers had on the overall structure.

Figure 5 to Figure 7 present the effect that reducing the input energy by 33, 66 and 100% (S1, S2 and S3) along with the number of layers (V1 to 9), had on the load bearing capacity of the structures. The results are also reported with the corresponding average TSD values, with associated max and min error bars. It can be seen from these graphs that as the level of deviation between the control data and the build data increased the compressive load (CL) of the parts decreased. This occurred due to the increasing number of layers with a reduction in energy input having an increasingly negative effect on the load bearing capacity, as well as having an increasing effect on the TSD value. Figure 7 shows the load bearing capacity of the S3 structures. As a number of these samples failed to recover from the layers processed with no

input energy, they failed to build successfully. The compressive load of these structures was therefor set to 0 N.

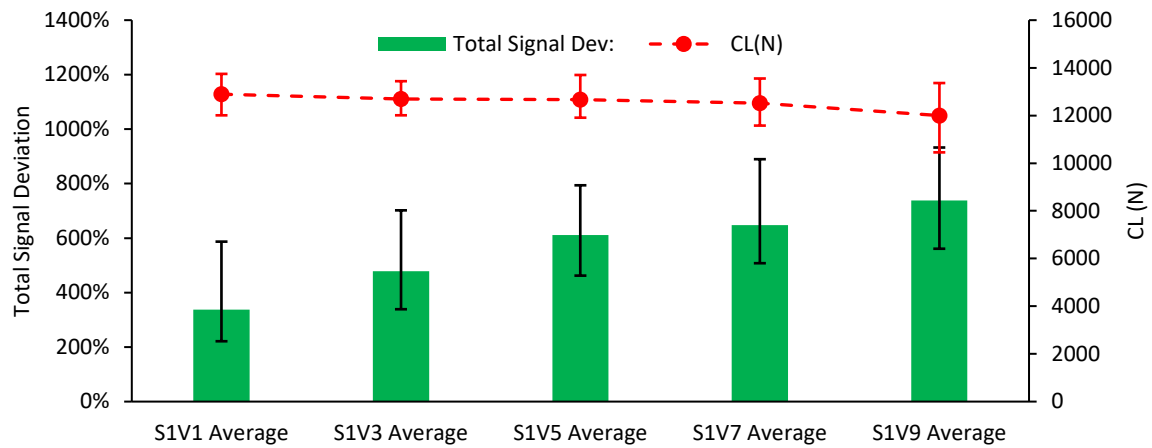


Figure 5: Correlation between signal deviation and part compressive load (CL), for parts created with an energy reduction of 33% (S1).

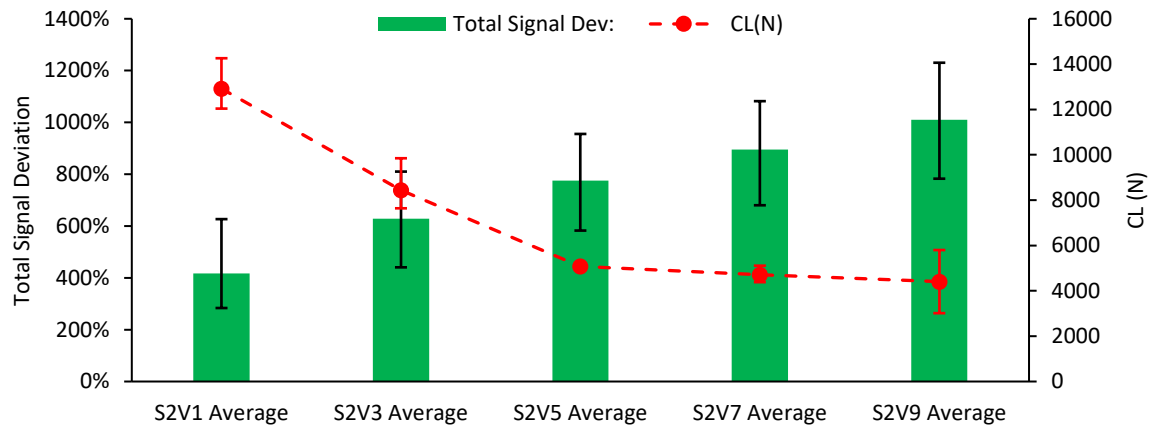


Figure 6: Correlation between signal deviation and part compressive load (CL), for parts created with an energy reduction of 66% (S2).

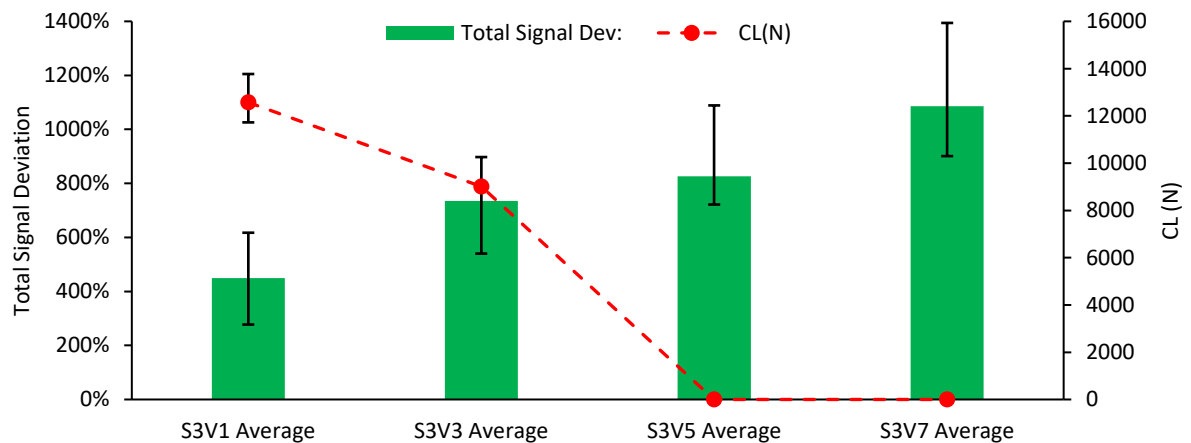


Figure 7: Correlation between signal deviation and part compressive load (CL), for parts created with an energy reduction of 100% (S3).

Figure 5 shows the effects that samples created with an energy reduction of 33% (S1) over the range of layers studied, had on the mechanical strength of the structures and on the TSD. It can be seen that the reduced input energy associated with this sample batch was sufficient to facilitate the formation of strut diameter close to that created by the control layers. Thus, the structures still exhibited mechanical strengths which were close to that of the control samples. A maximum reduction in load bearing capacity of 10% been obtained for the S1V9; however, a two way t-test demonstrated that there was no statistical difference between this sample group and the control sample group, for which no reduction in laser energy was applied ( $p=0.24$ ). The effect of processing these reduced input energy layers on the PM data generated can also be seen in Figure 5. It was observed that as the number of reduced energy input layers increased, an increase in the TSD, from 337% to 738%, was also observed, indicating that the correlation exists between the number of layers effected and the TSD value.

Figure 6 provides details on the effect of a 66 % (S2) reduction in laser energy. It is clear from this figure that the reduction in compressive load is significantly more rapid compared to that obtained for the 33% reduction in Figure 5. For example, when the energy input was reduced for 9 layers (S2V9), the mechanical strength of the structure reduced to just 3014 N, a of 67% reduction from the control sample. This is lower compared to the 10454 N obtained for the S1V9 structure, yielding a reduction of 10% from the control sample. Similarly, the TSD associated with these samples increased from 738%, for the S1V9 sample to 1010% for the S2V9 sample. This increased reduction in part strength is associated with the greater reduction in input energy associated with the S2 samples, leading to the formation of struts with significantly smaller strut diameters been formed, compared to that formed during the processing of the S1 samples. This increased reduction in input energy over each of the layers also resulted in an increase in the TSD value.

Figure 7 presents the results associated with the 100% (S3) laser energy reduction samples. Similar to the results observed in Figure 5 and 6, as the number of reduced input energy layers increased, so too did the TSD. Along with this, as the number of reduced energy input layers increased the load bearing capacity of the structures decreased dramatically. The S3 sample batch contained layers that were processed with no energy input, however the S3V1 and S3V3 samples built successfully. A probable explanation for this is that these structures built due to the energy input from the subsequent layers, processed with no reduction in input energy, been sufficient enough to melt through the unprocessed layers and bond to the structure below. As the number of unprocessed layers increased however, for example in the case of the S3V5 and S3V7 samples, based on the compressive load performance, the laser energy appeared to be

insufficient for adequate bonding between the struts to occur. Nevertheless, even though the 100% laser energy reduction S3V1 and S3V3 samples built successfully, the presence of the unprocessed layers still had a significant negative effect on the structures mechanical properties, with a reduction in the compressive load of 6% and 33% obtained respectively.

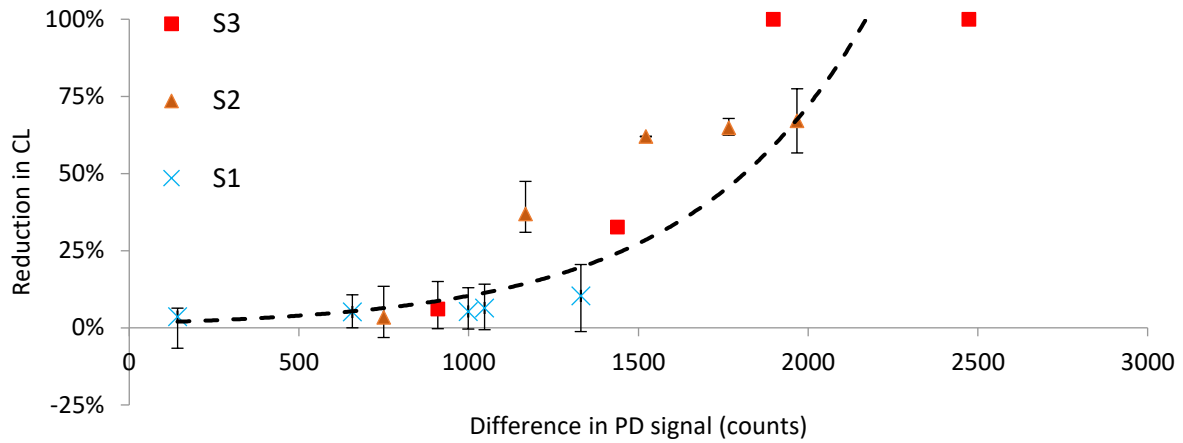


Figure 8: Reduction in compressive load (CL) of the structures containing low input energy layers, vs. the difference between the control samples PD signal and the samples containing low input energy layers PD signal.

The difference between the PD signal obtained from each of the samples containing low input energy layers and that of the control samples is plotted in Figure 8, against the reduction in compressive load exhibited by each. This reduction was obtained by calculating the difference in compressive load between the control samples and the samples containing low input energy layers. This result shows that at low signal deviation ( $< 891$  counts), a maximum reduction in compressive load of 6% was obtained. However, as the deviation between the respective data sets increased, due to an increase in the amount of low input energy layers and/or the increase in the level of input energy reduction, the reduction in part compressive load also increases. This result indicates that a correlation exists between the reduction in the compressive load of the structures and the deviation between the control samples and the build data's respective PD signals.

The 66% laser energy reduction S2V3 sample, with ~1200 counts difference, exhibited a 37% reduction in compressive load. This appears to be a significantly higher reduction in compressive load for the given signal deviation obtained. This is thought to have occurred due to the following reason. Compared to any of the 33% (S1) laser energy reduction samples the S2V1 sample and the S2V3 sample experienced a significant change in strut formation due to the presence of the reduced input energy layers. This can be seen in Figure 9, whereby the layers in the S2V3 sample with reduced input energy formed struts that may have acted as a weak point and a stress concentration point. This ultimately leads to a more severe reduction in part strength, compared to the other samples with similar PD signal deviation.



### 3.4 STRUT FORMATION & FAILURE MODE CHARACTERISATION

Having demonstrated the reduction in compressive strength associated with a reduction in laser input energy, this section investigates the effect of altering the laser power on strut formation.

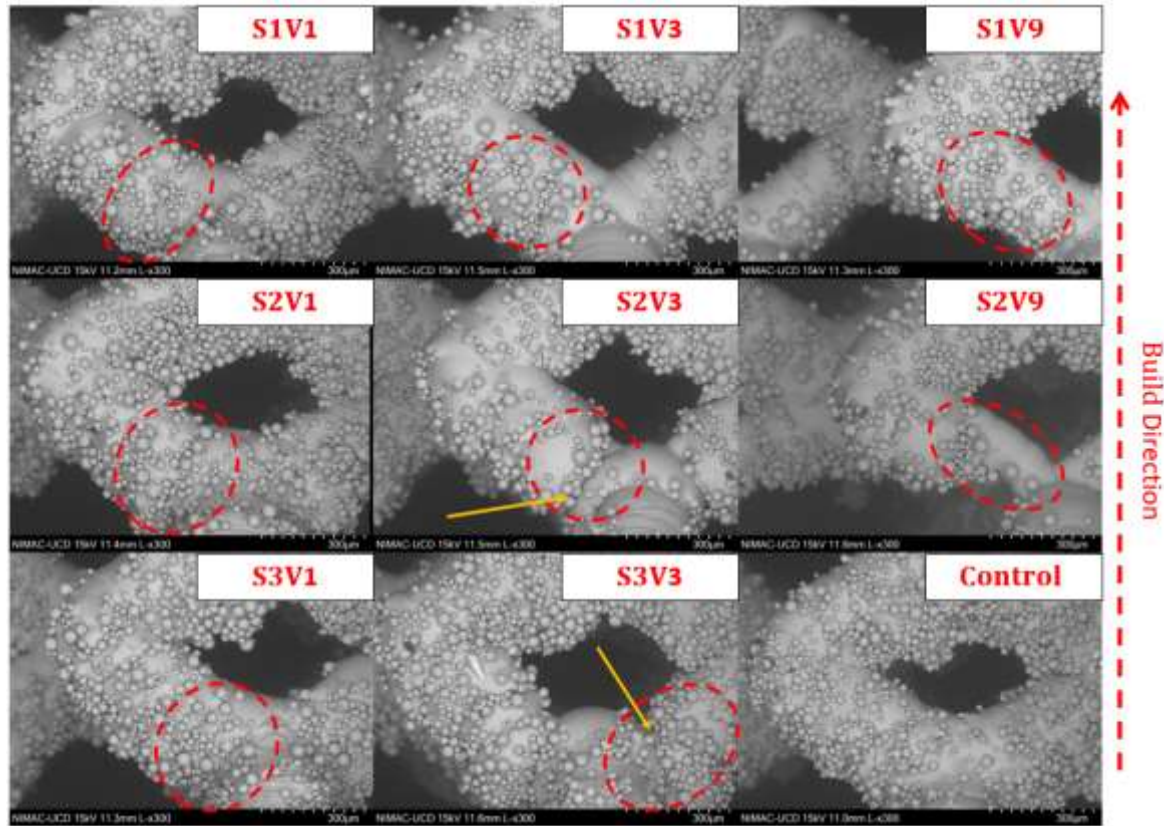


Figure 9: SEM images highlighting the effect that reducing the input energy had on the struts created. Also shown is the control sample (DF), bottom right.

High resolution SEM images were used to provide detailed visual information regarding the structural integrity of the as-built structures. Based on an examination of these images, strut measurements were taken from all 15 sample types. It was demonstrated that the average strut diameter was  $363 \pm 21 \mu\text{m}$ . The red circles highlighted in the SEM images given in Figure 9, highlight the discontinuities in the strut diameters when reduced energy input was applied during the build process. The yellow arrows highlight examples of necking phenomenon that also arose due to the reduced input energy layers. The reduction in strut diameter which is clearly observed for the S2V9 sample for example, clearly demonstrates how reducing input energy clearly effected strut formation. As anticipated this reduction is associated with a reduction in the load bearing capacity of the structures, as discussed previously. This figure demonstrates, that regardless of the level of input energy reduction, when the number of reduced input energy layers was just one (V1), there was little or no effect on the struts formed. The minimal effect that processing one layer with reduced, or no input energy (S1V1, S2V1



and S3V1) on the struts formed, and on the mechanical response of the structure, is thought to be due to the following reasons. During the processing of single layers with reduced laser energy of 33, 66, and 100% (the S1V1, the S2V1 and the S3V1), the subsequent layers provided enough input energy to negate the presence of the reduced input energy layer. Thus, the reduced input energy layer has a minimal effect on the mechanical strength of the structures. However, as the number of reduced input energy layers increased, this negative effect could not be completely corrected for by the powder melting which occurs during the processing of subsequent layers, resulting in the samples with the greater number of reduced input energy layers having an increasing effect on the load bearing capacity of the structures.

As the number of reduced input energy layers increased, for the S1 and S2 sample batches, the effect on the struts became more prominent. In the case of the 33% (S1) sample batch, as the number of reduced input energy layers increased from 1 to 9, the diameter of the struts created within these layers exhibited smaller diameters than obtained throughout the remainder of the structure. This occurred due to the lower input energy producing smaller strut diameters. As a result of this marginal decrease in strut diameter, only a small decrease in the load bearing capacity of these structures (S1V1 to S1V9) was obtained. In the case of the (66%) S2 samples, as the number of reduced input energy layers increased from 1 to 3, a small portion of the strut was created with a considerably smaller diameter than the control struts. This smaller strut diameter provided a potential crack propagation site (indicated by the arrow in Figure 9), both these phenomena resulted in the structure having a lower load bearing capacity than the control sample, with a reduction of 37% been obtained. As the number of reduced input energy layers further increased to 9, these effects were further amplified resulting in the structures load bearing capacity been reduced by 67%.

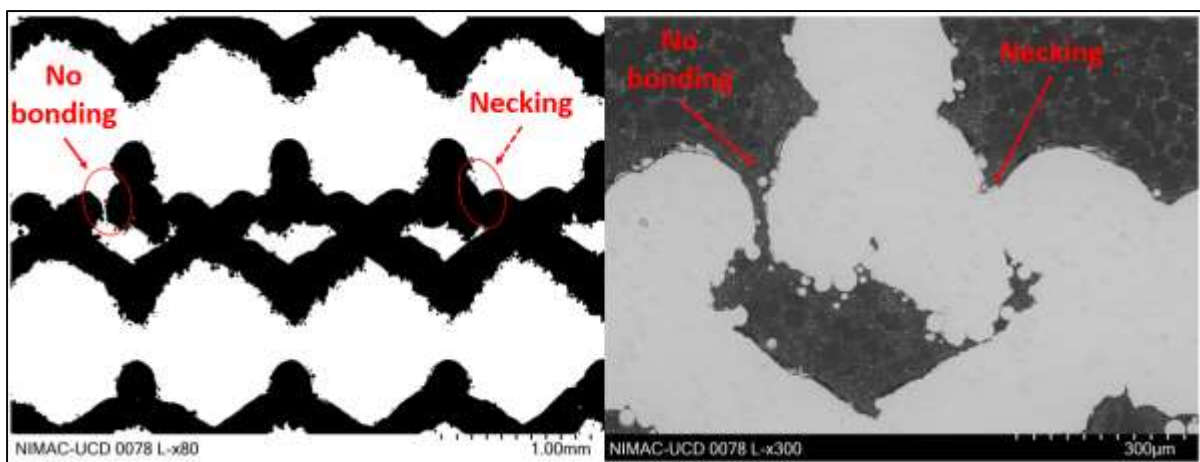
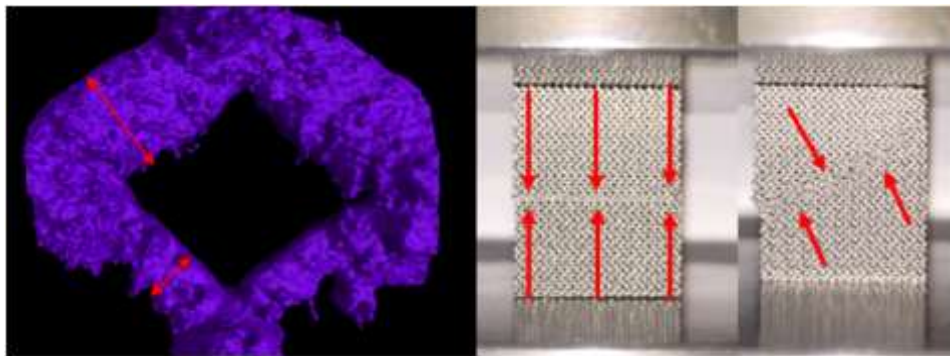


Figure 10: Left: Binary SEM image of a polished S3V3 structure, indicating areas of severe interlayer necking and areas where no interlayer bonding occurred. Right: SEM image of node junction indicating areas of no interlayer bonding, necking and the location where an increase meltpool depth occurred.

In the case of the samples with 100% reduced input energy (S3), as the number of layers with reduced input energy increased from 1 to 3, the presence of interlayer necking was observed. This in turn may have given rise for a crack propagation site to occur (arrow in Figure 9). In the case of the sample with a single 100% reduced input energy layer (S3V1), the energy input applied by the subsequent layer was sufficient to melt the powder below the unprocessed layer and thus bonding occurred. In this situation however where there was three layers with 100% reduced input energy (S3V3), there was insufficient energy applied in the subsequent layers to fully penetrate the thick powder layer ( $\sim 90 \mu\text{m}$  thick) and as a result little or no interlayer bonding occurred. This resulted in severe interlayer necking, and in some cases no interlayer bonding, occurring. Figure 10 left shows a binary SEM image of the ground and polished S3V3 sample, where the reduced input energy layers occurred. It is clear to see from this image where both the interlayer necking and the areas where no interlayer bonding occurred within the struts. Figure 10 right shows a close up view of one of the node junctions where both these phenomena occurred. As a result, the S3V3 samples possessing a significantly lower load bearing capacity than the control sample, with a 33% reduction in load bearing capacity been obtained.



*Figure 11: Left: CT scan of S2V9 sample highlighting struts processed with reduced input energy. Centre: Failure mode of S2V9 sample, showing “collapse” failure mode occurring at location where reduced energy input layers were processed. Right: Failure mode of the control sample, showing shear-band failure mode occurring.*

A  $\mu\text{CT}$  image of the as-built strut obtained with a 66% reduction in input energy over 9 layers (S2V9), demonstrates the reduced strut thickness which occurs associated with the use of reduced laser energy (Figure 11 left). The results shown in Figure 11 (centre and right), demonstrate the effect that the presence of these reduced input energy layers had on the failure mode of the structures created, after mechanical testing was carried out. As mentioned previously the samples with lower number of reduced input energy layers, regardless of the level of reduction, failed in a similar manner to the control samples due to the minimal effect that the reduced input energy layers had on the structures overall integrity. These samples, along with the control samples, failed with a shear band forming throughout the structure,

followed by layer-by-layer crushing along the band. This observation is in agreement with other published literature [33].

When the number of reduced input energy layers increased however, the structures failed in a ‘collapse’ like manner. A likely explanation for this collapse failure mode is that the smaller strut diameters, act as a potential crack propagation site (Figure 10). As the load bearing capacity of these layers is reduced, they fail prior to the larger strut diameters, resulting in a change in the observed failure mode.

## 4 CONCLUSIONS

In this study a Renishaw 500M system equipped with in-line photodiode (PD) based process monitoring capability, was used to create Ti-6Al-4V porous structures using the single exposure method. The photodiode data generated during processing of control samples was compared to the data generated during processing of the porous structures containing layers with reduced energy input. The number of layers containing reduced energy input was varied between 1 and 9, while the energy reduction within those layers varied between 33%, 66% and 100 %, of that used in the control sample. The effect this had on both the load bearing capacity of the structures and on the process monitoring data generated during the SLM process, was analysed. It was shown that at each of the energy input reduction levels studied, as the number of low input energy layers increased, the load bearing capacity of the structures decreased. Associated with the increasing number of low input energy layers was an increase in difference between the control samples PD signal and the signal generated by the samples containing the low input energy layers.

This study for the first time demonstrates a correlation between the load bearing capacity of porous structures and in-situ process monitoring data. The change in PD signal with reduced laser energy was directly correlated with a reduction in the load bearing capacity of porous structures. By comparing build data when reduced laser energy was applied, to control data, valuable process monitoring information relating to the structural integrity of the porous could be determined. The sensitivity of the mechanical response of the structures and the PM system to layers processed with a reduction in input energy, was demonstrated. For example, when 3 layers, containing a 33% reduction in input energy was processed, the structures exhibited a 5% reduction in compressive load, compared to the control. A very similar compressive load reduction of 6%, was obtained with a single layer with no power applied (reduction of 100%). When 5 layers with a 66% reduced input energy layers was applied, the reduction in load

bearing capacity was 62%. It is important to stress however, that the performance of any given structure will be dependent on a number of factors, such as part geometry, and the level of input energy used in the subsequent layers.

## ACKNOWLEDGEMENT

This publication has emanated from research supported in part by a research grant from Science Foundation Ireland (SFI) under Grant Number 16/RC/3872 and is co-funded under the European Regional Development Fund. The authors would also like to acknowledge the technical assistance and support provided by Croom Precision Medical Ltd.

## BIBLIOGRAPHY

- [1] S. Van Bael, Y.C. Chai, S. Truscetto, M. Moesen, G. Kerckhofs, H. Van Oosterwyck, J.P. Kruth, J. Schrooten, The effect of pore geometry on the in vitro biological behavior of human periosteum-derived cells seeded on selective laser-melted Ti6Al4V bone scaffolds, *Acta Biomater.* 8 (2012) 2824–2834. doi:10.1016/j.actbio.2012.04.001.
- [2] L. Xiao, W. Song, Additively-manufactured functionally graded Ti-6Al-4V lattice structures with high strength under static and dynamic loading: Experiments, *Int. J. Impact Eng.* 111 (2018) 255–272. doi:10.1016/j.ijimpeng.2017.09.018.
- [3] D.S.J. Al-Saedi, S.H. Masood, M. Faizan-Ur-Rab, A. Alomarah, P. Ponnusamy, Mechanical properties and energy absorption capability of functionally graded F2BCC lattice fabricated by SLM, *Mater. Des.* 144 (2018) 32–44. doi:10.1016/j.matdes.2018.01.059.
- [4] G. Lewis, Properties of open-cell porous metals and alloys for orthopaedic applications, *J. Mater. Sci. Mater. Med.* 24 (2013) 2293–2325. doi:10.1007/s10856-013-4998-y.
- [5] A.M. Khorasani, I. Gibson, U.S. Awan, A. Ghaderi, The effect of SLM process parameters on density, hardness, tensile strength and surface quality of Ti-6Al-4V, *Addit. Manuf.* 25 (2019) 176–186. doi:10.1016/j.addma.2018.09.002.
- [6] W. Xu, M. Brandt, S. Sun, J. Elambasseril, Q. Liu, K. Latham, K. Xia, M. Qian, Additive manufacturing of strong and ductile Ti-6Al-4V by selective laser melting via in situ martensite decomposition, *Acta Mater.* 85 (2015) 74–84. doi:10.1016/j.actamat.2014.11.028.
- [7] F. R. Kaschel, M. Celikin, D.P. Dowling, Effects of laser power on geometry, microstructure and mechanical properties of printed Ti-6Al-4V parts, *J. Mater. Process. Technol.* 278 (2020) 116539. doi:10.1016/j.jmatprotec.2019.116539.
- [8] D. Melancon, Z.S. Bagheri, R.B. Johnston, L. Liu, M. Tanzer, D. Pasini, Mechanical characterization of structurally porous biomaterials built via additive manufacturing : experiments , predictive models , and design maps for load-bearing bone replacement implants, *Acta Biomater.* 63 (2017) 350–368. doi:10.1016/j.actbio.2017.09.013.
- [9] F.S.L. Bobbert, K. Lietaert, A.A. Eftekhari, B. Pouran, S.M. Ahmadi, H. Weinans, A.A. Zadpoor, Additively manufactured metallic porous biomaterials based on minimal surfaces: A unique combination of topological, mechanical, and mass transport properties, *Acta Biomater.* 53 (2017) 572–584. doi:10.1016/j.actbio.2017.02.024.
- [10] M. Dallago, V. Fontanari, E. Torresani, M. Leoni, C. Pederzoli, C. Potrich, M. Benedetti, Fatigue and biological properties of Ti-6Al-4V ELI cellular structures with

- variously arranged cubic cells made by selective laser melting, *J. Mech. Behav. Biomed. Mater.* 78 (2018) 381–394. doi:10.1016/j.jmbbm.2017.11.044.
- [11] H. Wang, S. Johnston, D. Rosen, Design of a graded cellular structure for an acetabular hip replacement component, *17th Solid Free. Fabr. (2006)* 111–123. doi:10.1088/1758-5082/6/4/045007.
  - [12] S.C. Cox, P. Jamshidi, N.M. Eisenstein, M.A. Webber, H. Hassanin, M.M. Attallah, D.E.T. Shepherd, O. Addison, L.M. Grover, Adding functionality with additive manufacturing: Fabrication of titanium-based antibiotic eluting implants, *Mater. Sci. Eng. C.* 64 (2016) 407–415. doi:10.1016/j.msec.2016.04.006.
  - [13] H. Hassanin, L. Finet, S.C. Cox, P. Jamshidi, L.M. Grover, D.E.T. Shepherd, O. Addison, M.M. Attallah, Tailoring selective laser melting process for titanium drug-delivering implants with releasing micro-channels, *Addit. Manuf.* 20 (2018) 144–155. doi:10.1016/j.addma.2018.01.005.
  - [14] P.-I. Tsai, C.-C. Hsu, S.-Y. Chen, T.-H. Wu, C.-C. Huang, Biomechanical investigation into the structural design of porous additive manufactured cages using numerical and experimental approaches, *Comput. Biol. Med.* 76 (2016) 14–23. doi:10.1016/j.compbimed.2016.06.016.
  - [15] B. Jetté, V. Brailovski, M. Dumas, C. Simoneau, P. Terriault, Femoral stem incorporating a diamond cubic lattice structure : Design , manufacture and testing, *J. Mech. Behav. Biomed. Mater.* 77 (2018) 58–72. doi:10.1016/j.jmbbm.2017.08.034.
  - [16] L. Mullen, R.C. Stamp, W.K. Brooks, E. Jones, C.J. Sutcliffe, Selective laser melting: A regular unit cell approach for the manufacture of porous, titanium, bone in-growth constructs, suitable for orthopedic applications, *J. Biomed. Mater. Res. - Part B Appl. Biomater.* 89 (2009) 325–334. doi:10.1002/jbm.b.31219.
  - [17] R.J. van Arkel, S. Ghouse, P.E. Milner, J.R.T. Jeffers, Additive manufactured push-fit implant fixation with screw-strength pull out, *J. Orthop. Res.* 36 (2018) 1508–1518. doi:10.1002/jor.23771.
  - [18] N. Taniguchi, S. Fujibayashi, M. Takemoto, K. Sasaki, B. Otsuki, Effect of pore size on bone ingrowth into porous titanium implants.pdf, *Mater. Sci. Eng. C.* 59 (2016) 690–701.
  - [19] D. Mahmoud, M. Elbestawi, Lattice Structures and Functionally Graded Materials Applications in Additive Manufacturing of Orthopedic Implants: A Review, *J. Manuf. Mater. Process.* 1 (2017) 13. doi:10.3390/jmmp1020013.
  - [20] S. Arabnejad, R. Burnett Johnston, J.A. Pura, B. Singh, M. Tanzer, D. Pasini, High-strength porous biomaterials for bone replacement: A strategy to assess the interplay between cell morphology, mechanical properties, bone ingrowth and manufacturing constraints, *Acta Biomater.* 30 (2016) 345–356. doi:10.1016/j.actbio.2015.10.048.
  - [21] F. Liu, D. Zhang, P. Zhang, M. Zhao, Mechanical Properties of Optimized Diamond Lattice Structure for Bone Scaffolds Fabricated via Selective, *Materials (Basel)*. 11 (2018). doi:10.3390/ma11030374.
  - [22] S.K. Everton, M. Hirsch, P. Stravroulakis, R.K. Leach, A.T. Clare, Review of in situ process monitoring and in situ metrology for metal additive manufacturing, *Mater. Des.* 95 (2016) 431–445. doi:http://dx.doi.org/10.1016/j.matdes.2016.01.099.
  - [23] S. Clijsters, T. Craeghs, S. Buls, K. Kempen, J.P. Kruth, In situ quality control of the selective laser melting process using a high-speed, real-time melt pool monitoring system, *Int. J. Adv. Manuf. Technol.* 75 (2014) 1089–1101. doi:10.1007/s00170-014-6214-8.
  - [24] G. Bi, C.N. Sun, A. Gasser, Study on influential factors for process monitoring and control in laser aided additive manufacturing, *J. Mater. Process. Technol.* 213 (2013) 463–468.

- [25] T. Craeghs, S. Clijsters, E. Yasa, J.-P. Kruth, Online quality control of selective laser melting, in: *Proc. Solid Free. Fabr. Symp.*, Austin, 2011: pp. 212–226.
- [26] S. Berumen, F. Bechmann, S. Lindner, J.-P. Kruth, T. Craeghs, Quality control of laser- and powder bed-based Additive Manufacturing (AM) technologies, *Phys. Procedia*. 5 (2010) 617–622. doi:10.1016/j.phpro.2010.08.089.
- [27] D. Alberts, D. Schwarze, G. Witt, In situ melt pool monitoring and the correlation to part density of Inconel 718 for quality assurance in selective laser melting, in: *Solid Free. Fabr. Proc.*, 2017.
- [28] J.A. Kanko, A.P. Sibley, J.M. Fraser, In situ morphology-based defect detection of selective laser melting through inline coherent imaging, *J. Mater. Process. Technol.* 231 (2016) 488–500. doi:10.1016/j.jmatprotec.2015.12.024.
- [29] M. Bisht, N. Ray, F. Verbist, S. Coeck, Correlation of selective laser melting-melt pool events with the tensile properties of Ti-6Al-4V ELI processed by laser powder bed fusion, *Addit. Manuf.* 22 (2018) 302–306. doi:10.1016/j.addma.2018.05.004.
- [30] Renishaw PLC, InfiniAM Spectral – Energy input and melt pool emissions monitoring for AM systems, Data Sheet. (2018) 1–5. <http://resources.renishaw.com/en/details/data-sheet-renam-500q--99032>.
- [31] D.S. Egan, D.P. Dowling, Influence of process parameters on the correlation between in-situ process monitoring data and the mechanical properties of Ti-6Al-4V non-stochastic cellular structures, *Addit. Manuf.* 30 (2019) 100890. doi:10.1016/j.addma.2019.100890.
- [32] B.M. Sharratt, Non-Destructive Techniques and Technologies for Qualification of Additive Manufactured Parts and Processes: A review, Sharratt Res. Consult. Inc. (2015).
- [33] J. Kadkhodapour, H. Montazerian, A.C. Darabi, A.P. Anaraki, S.M. Ahmadi, A.A. Zadpoor, S. Schmauder, Failure mechanisms of additively manufactured porous biomaterials: Effects of porosity and type of unit cell, *J. Mech. Behav. Biomed. Mater.* 50 (2015) 180–191. doi:10.1016/j.jmbbm.2015.06.012.